

A Transfer-Learning Approach for Accelerated MRI using Deep Neural Networks

Salman UI Hassan Dar^{1,2}, Tolga Çukur^{1,2,3}

¹Department of Electrical and Electronics Engineering, Bilkent University, Ankara, Turkey

²National Magnetic Resonance Research Center (UMRAM), Bilkent University, Ankara, Turkey

³Neuroscience Program, Sabuncu Brain Research Center, Bilkent University, Ankara, Turkey

Running title: A transfer-learning approach for accelerated MRI using deep neural networks.

Address correspondence to:

Tolga Çukur

Department of Electrical and Electronics Engineering, Room 304

Bilkent University

Ankara, TR-06800, Turkey

TEL: +90 (312) 290-1164

E-MAIL: cukur@ee.bilkent.edu.tr

This work was supported in part by a Marie Curie Actions Career Integration Grant (PCIG13-GA- 2013-618101), by a European Molecular Biology Organization Installation Grant (IG 3028), by a TUBA GEBIP fellowship, and by a BAGEP fellowship awarded to T. Çukur.

We also gratefully acknowledge the support of NVIDIA Corporation with the donation of the Titan X Pascal GPU used for this research.

Abstract

Neural network based architectures have recently been proposed for reconstruction of undersampled MR acquisitions. A deep network containing many free parameters is typically trained using a relatively large set of fully-sampled MRI data, and later used for on-line reconstruction of undersampled data. Ideally network performance should be optimized by drawing the training and testing data from the same domain. In practice, however, large datasets comprising hundreds of subjects scanned under a common protocol are rare. Here, we propose a transfer-learning approach to address the problem of data scarcity in training deep networks for accelerated MRI. The proposed approach trains neural networks using thousands of samples from a public dataset of natural images (ImageNet). The network is then fine-tuned using only few tens of MR images acquired in the testing domain (T1- or T2-weighted MRI). The ImageNet-trained network yields nearly identical reconstructions to networks trained directly in the testing domain using thousands of MR images, and it outperforms conventional compressed sensing reconstructions in terms of image quality. The proposed approach might facilitate the use of neural networks for MRI reconstruction without the need for collection of extensive imaging datasets.

1 - Introduction

The unparalleled soft-tissue contrast in MRI has rendered it a preferred modality in many diagnostic applications, but long scan durations limit its clinical use. Acquisitions can be accelerated by undersampling in k-space, and a tailored reconstruction can be used to recover unacquired data. Because MR images are inherently compressible, a popular framework for accelerated MRI has been compressive sensing (CS) [1], [2]. CS has offered improvements in scan efficiency in many applications including structural [2], angiographic [3], functional [4], diffusion [5], and parametric imaging [6]. Yet the CS framework is not without limitation. First, CS involves nonlinear optimization algorithms that scale poorly with growing data size and hamper clinical workflow. Second, CS commonly assumes that MRI data are sparse in fixed transform domains, such as finite differences or wavelet transforms. Recent studies highlight the need for learning the transform domains specific to each dataset to optimize performance [7]. Lastly, CS requires careful parameter tuning (e.g., for regularization) for optimal performance. While several approaches were proposed for data-driven parameter tuning [8], [9], these methods can induce further computational burden.

Neural network (NN) architectures that reconstruct images from undersampled data have recently been proposed to address the above limitations [10]–[19]. A network is trained off-line using a relatively large set of fully-sampled MRI data, and the trained network is later used for on-line reconstruction of undersampled data. Reconstructions can be achieved in several hundred milliseconds, significantly reducing computational burden [12]–[16], [18]. The NN framework also alleviates the need for adhoc selection of transform domains. For example, an early study replaced explicit sparsity constraints in CS with the output of a four-layered convolutional neural network (CNN) that was trained to learn the mapping from zero-filled Fourier reconstructions of undersampled data to fully sampled images [10]. In other studies, a cascade of CNNs were used that were trained to recover images from zero-filled reconstructions of undersampled data [12], [13], [15]. In both cases, the trained networks automatically learn suitable transforms for image reconstruction. The NN framework introduces more tunable hyperparameters (e.g., number of layers, units, activation functions) than would be required in CS. However, previous studies demonstrate that hyperparameters optimized during the training phase generally perform well in the testing phase [10]–[19]. Taken together, these advantages render the NN framework a promising avenue for accelerated MRI.

A common strategy to enhance network performance is to increase the number of layers and units in the architecture. A large set of training data must then be used to reliably learn the numerous network parameters [20]. Previous studies either used an extensive database of MR images comprising several hundreds of subjects [14], [16], [17], or data augmentation procedures to artificially expand the size of training data [12], [14]. For instance, an early study performed training on T1-weighted brain images from nearly 500 subjects in the human connectome project (HCP) database, and later tested the NN on T2-weighted images [17]. That said, it remains unclear how well a network trained on images acquired with a specific type of tissue contrast generalize to images acquired with different contrasts. Furthermore, for optimal reconstruction performance the network must be trained on images acquired with the same scan protocol that it later will be tested on. Unfortunately, large databases such as those provided by the HCP may not be readily available in many applications, rendering NN-based reconstructions suboptimal.

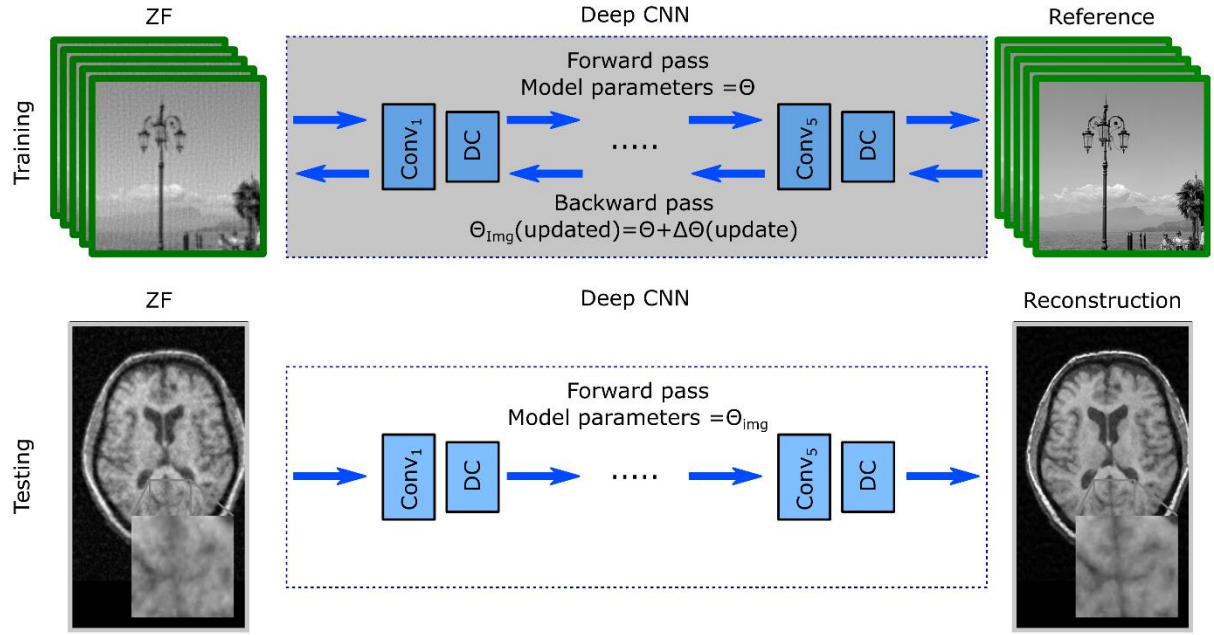
In this study, we propose a transfer-learning approach to address the problem of data scarcity in network training for accelerated MRI. In transfer-learning, network training is performed in some domain where large datasets are available, and knowledge captured by the trained network is then transferred to a different domain where the dataset is sizably small [21], [22]. Domain transfer was previously used to suppress coherent aliasing artifacts in projection reconstruction acquisitions [11], and to perform non-Cartesian to Cartesian interpolation in k-space [17]. Here, we instead employ transfer-learning to enhance NN-based reconstructions of variably-density randomly undersampled acquisitions. The proposed approach uses a deep CNN architecture with multiple subnetworks [12]. In the training domain using several thousand images, each subnetwork is trained sequentially to reconstruct reference images from zero-filled reconstructions of undersampled data. The full network is then fine-tuned end-to-end in the testing domain using few tens of images. With this approach, we demonstrate successful domain transfer between MR images acquired with different contrasts (T1- and T2-weighted images), and between natural and MR images (ImageNet and T1- or T2-weighted images). We show that networks obtained via transfer-learning using only tens of images in the testing domain achieve nearly identical performance to networks trained directly in the testing domain using thousands of images.

Contributions

Following are our contributions:

1. We demonstrate a transfer-learning approach for accelerated MRI that efficiently trains neural networks using a relatively small number of data samples in the testing domain.
2. We show that a deep cascade of CNNs for MRI reconstruction can be trained using natural images on ImageNet, and then fine-tuned using as few as 10-20 MR images, and that this network can successfully recover unacquired data for acceleration factors up to 4.
3. We show that a network trained on MR images with a first contrast (e.g., T1-weighted) yields suboptimal performance in reconstructing images acquired with a second contrast (e.g., T2-weighted).
4. We show that, after fine tuning using as few as 20 images, a network trained on images with the first contrast performs comparably to an optimal network trained on images with the second contrast.
5. We also show that this proposed transfer-learning approach outperforms conventional CS reconstructions in terms of image quality.

a) Imagenet-trained network



b) Domain transfer to T1-weighted images

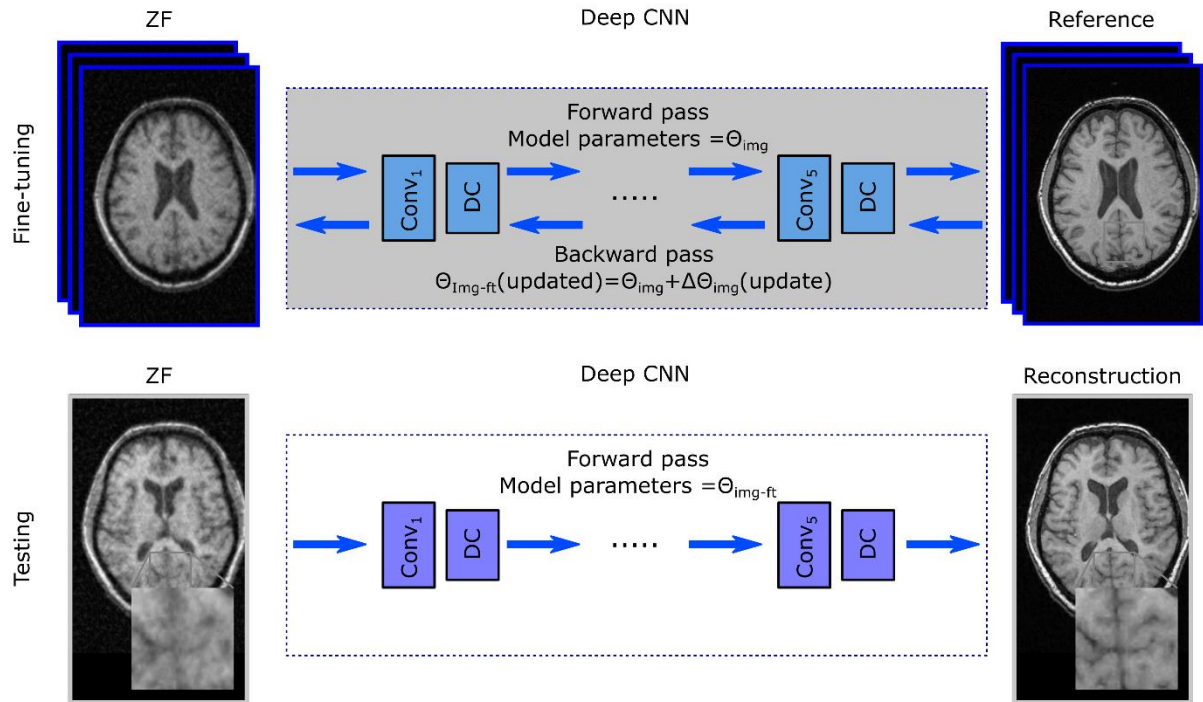


Figure 1. Proposed transfer-learning approach for NN-based reconstructions of variably-density undersampled acquisitions. A deep architecture with multiple subnetworks is used. The subnetworks consist of a CNN block “Conv” followed by a data consistency block “DC”. (a) Each subnetwork is trained sequentially to reconstruct natural images from the ImageNet database, given zero-filled Fourier reconstructions of their undersampled versions. Due to differences in the characteristics of natural and MR images, the ImageNet-trained network will yield suboptimal performance when tested on MR images. (b) For domain transfer, the ImageNet-trained network is fine-tuned end-to-end in the testing domain using few tens of images. This approach enables successful domain transfer between natural and MR images.

2 – Methods

2.1 - Problem formulation

2.1.1 –MRI Reconstruction via Compressed Sensing (CS)

In accelerated MRI, an undersampled acquisition is followed by a reconstruction to recover missing k-space samples. This recovery can be formulated as a linear inverse problem:

$$F_u x = y_u \quad (1)$$

where x denotes the image to be reconstructed, F_u is the partial Fourier transform operator at the sampled k-space locations, and y_u denotes acquired k-space data. Since Eq. 1 is underdetermined, additional prior information is typically incorporated in the form of a regularization term:

$$\min_x \|F_u x - y_u\|_2 + R(x) \quad (2)$$

Here, the first term enforces consistency between acquired and reconstructed data, whereas $R(x)$ enforces prior information to improve reconstruction performance. In CS, $R(x)$ corresponds to the L_0 or L_1 norm of the image in a known transform domain (e.g., wavelet transform or finite differences transform).

The solution of Eq. 2 involves non-linear optimization algorithms that are often computationally complex. This reduces clinical feasibility as reconstructions times become prohibitive with increasing size of data. Furthermore, assuming ad hoc selection of fixed transform domains leads to suboptimal reconstructions in many applications [7]. Lastly, it is challenging to find a set of reconstruction parameters that work optimally across subjects.

2.1.2 – MRI Reconstruction via Neural Networks (NN)

In the NN framework for accelerated MRI, a network architecture is used for reconstruction instead of explicit transform-domain constraints. Network training is performed via a supervised learning procedure, with the aim to find the set of network parameters that yield accurate reconstructions undersampled acquisitions. This procedure is performed on a large set of training data (with N_{train} samples), where fully-sampled reference acquisitions are retrospectively undersampled. Network training typically amounts to minimizing the following loss function [10]:

$$\min_{\theta} \sum_{n=1}^{N_{train}} \frac{1}{N_{train}} \|C(x_{un}; \theta) - x_{refn}\|_2 \quad (3)$$

where x_{un} represents the Fourier reconstruction of n^{th} undersampled acquisition, x_{refn} represents the respective Fourier reconstruction of the fully-sampled acquisition, $C(x_{un}; \theta)$ denotes the output of the network given the input image x_{un} and the network parameters θ . To reduce sensitivity to outliers, here we minimized a hybrid loss that includes both mean-squared error and mean-absolute error terms. To minimize over-fitting, we further added an L2-regularization term on the network parameters. Therefore, neural network training was performed with the following loss function:

$$\min_{\theta} \sum_{n=1}^{N_{train}} \frac{1}{N_{train}} \|C(x_{un}; \theta) - x_{refn}\|_2 + \sum_{n=1}^{N_{train}} \frac{1}{N_{train}} \|C(x_{un}; \theta) - x_{refn}\|_1 + \gamma_{\Phi} \|\theta\|_2 \quad (4)$$

where γ_ϕ is the regularization parameter for the network parameters.

A network trained on a sufficiently large set of training examples can then be used to reconstruct an undersampled acquisition from an independent test dataset. This reconstruction can be achieved by reformulating the problem in Eq. 2 [10]:

$$x_{rec} = \min_x \lambda \|F_u x - y_u\|^2 + \|C(x_u; \theta^*) - x\|^2 \quad (5)$$

where $C(x_u; \theta^*)$ is the output of the trained network with optimized parameters θ^* . Note that the problem in Eq. 5 has the following closed-form solution [10].

$$y_{rec}(k) = \begin{cases} \frac{F\{C(x_u; \theta^*)\}(k) + \lambda y_u(k)}{1 + \lambda}, & \text{if } k \in \Omega \\ F\{C(x_u; \theta^*)\}(k), & \text{otherwise} \end{cases} \quad (6)$$

$$x_{rec} = F^{-1}\{y_{rec}\}$$

where k denotes k -space location, Ω represents the set of acquired k -space locations, F and F^{-1} are the forward and backward Fourier transform operators, and x_{rec} is the reconstructed image. The solution outlined in Eq. 6 performs two separate projections during reconstruction. The first projection calculates the output of the trained neural network $C(x_u; \theta^*)$ given the input image x_u , the Fourier reconstruction of undersampled data. The second projection enforces consistency between the acquired and reconstructed k -space data. The parameter λ in Eq. 6 controls the relative weighing between data samples that are originally acquired and those that are recovered by the network. Here we used $\lambda = \infty$ to enforce data consistency strictly by replacing the network-recovered data samples with their original values. The data-consistency projection outlined in Eq. 6 can be compactly expressed as [12]:

$$f_{DC}\{C(x_u; \theta^*)\} = F^{-1}\{\Lambda F\{C(x_u; \theta^*)\}\} + \frac{\lambda}{1 + \lambda} F^{-1}\{x_u\} \quad (7)$$

where Λ is a diagonal matrix with diagonal terms:

$$\Lambda_{kk} = \begin{cases} \frac{1}{1 + \lambda}, & \text{if } k \in \Omega \\ 1, & \text{otherwise} \end{cases} \quad (8)$$

Conventional optimization algorithms for CS run iteratively to progressively minimize the loss function. A similar approach can also be adopted for NN-based reconstructions [12], [13], [15]. Here, we cascaded several sub-networks in series with data-consistency projections interleaved between consecutive sub-networks [12]. In this architecture, the input x_{ip} to the p^{th} sub-network was formed as:

$$x_{ip} = \begin{cases} x_{un}, & \text{if } p = 1 \\ f_{DC}\{C_{p-1}(f_{DC}\{C_{p-2}(f_{DC} \dots C_1(x_{un}; \theta_1^*); \theta_{p-1}^*)\}), & \text{if } p > 1 \end{cases} \quad (9)$$

Where θ_p^* denotes the parameters of the p^{th} subnetwork. Starting with the initial network with $p = 1$, each subnetwork was trained sequentially by solving the following optimization problem:

$$\min_{\theta_p} \sum_{n=1}^{N_{train}} \frac{1}{N_{train}} \|C(x_{ip}; \theta_p) - x_{refn}\|_2 + \sum_{n=1}^{N_{train}} \frac{1}{N_{train}} \|C(x_{ip}; \theta_p) - x_{refn}\|_1 + \gamma_\phi \|\theta_p\|^2 \quad (10)$$

While training the p^{th} subnetwork, the parameters of preceding networks and thus the input x_{ip} are assumed to be fixed.

2.2 - Datasets

Three distinct datasets of images were used in this work to train neural-networks: natural images, T1-weighted MR images, and T2-weighted MR images. The details of the datasets are listed below.

1 – Natural images: For training NNs, we assembled 4000 natural images from the validation set used during the ImageNet Large Scale Visual Recognition Challenge 2011 (ILSVRC2011) [23]. All images were either cropped or zero-padded to yield consistent dimensions of 256x256. Color RGB images were first converted to LAB color space, and the L-channel was extracted to obtain grayscale images.

2 – T1-weighted images: For training NNs, we assembled a total of 4000 T1-weighted images (34 subjects) from the MIDAS database [24]. A distinct set of 628 images (5 subjects) from the same dataset were reserved for testing the trained networks. The T1-weighted images analyzed here were collected on a 3T scanner via the following parameters: a 3D gradient-echo sequence, TR=14ms, TE=7.7ms, flip angle=25°, matrix size=256x176, 1 mm isotropic resolution.

3 – T2-weighted images: For training NNs, we assembled a total of 4000 T2-weighted images (32 subjects) from the MIDAS database [24]. A distinct set of 640 images (5 subjects) from the same dataset were reserved for testing the trained networks. The T2-weighted images analyzed here were collected on a 3T scanner via the following parameters: a 2D spin-echo sequence, TR=7730ms, TE=80ms, flip angle=180°, matrix size=256x192, 1 mm isotropic resolution.

We trained three separate networks using the aforementioned datasets. The first network was trained on natural images from ImageNet (ImageNet-trained network), the second network was trained on T1-weighted images from MIDAS (T1-trained network), and the third network was trained on T2-weighted images from MIDAS (T2-trained network).

Images in each dataset were undersampled via variable-density Poisson-disc sampling [25]. An acceleration factor of 4x was prescribed for all analyses reported in this study. Note that the undersampling masks for natural, T1-weighted, and T2-weighted images were slightly different due to intrinsic differences in image sizes. To ensure reliability against mask selection, 100 unique undersampling masks were generated and used during the training phase. A different set of 100 undersampling masks were used during the testing phase.

2.3 - Network training

For reconstructing undersampled acquisitions, we adopted a cascade of neural networks interleaved by data-consistency layers, an architecture inspired by [12]. Five sub-networks were cascaded in series. Each sub-network contained an input layer, four convolutional layers and an output layer. The input layer consisted of two channels, one for the real part and one for the complex part of the undersampled images. Each convolution operation in the convolutional layers was passed through a rectified linear unit (ReLU) activation function.

The hidden layers consisted of 64 channels. The output layer consisted of only a single channel for a magnitude reconstruction.

2.3.1 - Sub-network training

The sub-networks were trained via the back-propagation algorithm [26]. In the forward passes, a batch of 50 samples were passed through the network to calculate the respective loss function. In the backward passes, network parameters were updated according to the gradients of this function with respect to the parameters. The gradient of the loss function with respect to parameters of the m^{th} hidden layer (θ_m) can be calculated using chain rule:

$$\frac{\partial L}{\partial \theta_m} = \frac{\partial L}{\partial o_l} \frac{\partial o_l}{\partial a_l} \frac{\partial a_l}{\partial \theta_l} \frac{\partial o_{l-1}}{\partial a_{l-1}} \dots \frac{\partial o_m}{\partial a_m} \frac{\partial a_m}{\partial \theta_m} \quad (11)$$

where l is the output layer of the network, a_l is the output of the l^{th} layer, and o_l is the output of the l^{th} layer passed through the activation function. The parameters of the m^{th} layer will only be updated if the loss-function gradient flows through all subsequent layers (is non-zero).

Each sub-network was trained individually for 20 epochs. In the training phase, the network parameters were optimized using the ADAM optimizer with a learning rate of $\eta=10^{-4}$, decay rate for first moment of gradient estimates of $\beta_1=0.9$ and decay rate for the second moment of gradient estimate of $\beta_2=0.999$ [27]. Connection weights were L2-regularized with a regularization parameter of $\gamma_\phi=10^{-6}$.

2.3.2 - Fine tuning

To enhance network performance, networks formed by sequential training of the subnetworks were fine tuned. Here, end-to-end fine tuning was performed on the entire neural-network architecture. To do this, the gradients must be calculated through both the sub-networks and the data-consistency layers. The gradient flow through the convolutional sub-networks that contain basic arithmetic operations and ReLU activation functions are well known. The gradient flow through the data-consistency layer expressed in Eq. 7 with respect to its input $C(x_u; \theta^*)$ is given as:

$$\frac{\partial f_{DC}}{\partial C(x_u; \theta^*)} = F^{-1} \Delta F \quad (12)$$

due to the linearity of the Fourier transform operator (F). During the fine-tuning phase, the ADAM optimizer was used with identical parameters to those used in sub-network training, apart from a lower learning rate of 10^{-5} and a total of 150 epochs.

2.3 – Performance analyses

First, we investigated how well the network trained on a given dataset generalizes to other types of datasets. We reasoned that a network trained on the same type of images that it will later be tested on should outperform networks trained on different types of images than those in the test set. To investigate this issue, we reconstructed undersampled T1-weighted acquisitions using the ImageNet-trained and T2-trained networks. The reconstructions obtained via these two networks were compared with reference reconstructions obtained from the network trained directly on T1-weighted images. To ensure that our results were not biased by the selection of a specific MR contrast as the test set, we also reconstructed undersampled T2-weighted acquisitions using the ImageNet-trained and T1-trained

networks. The reconstructions obtained via these two networks were compared with reference reconstructions obtained from the network trained directly on T2-weighted images.

Next, we examined the success of the proposed transfer-learning approach in NN-based reconstructions. To do this, we performed end-to-end fine-tuning of networks in the testing domain. When T1-weighted images were selected as the testing domain, ImageNet-trained and T2-trained networks were fine-tuned using a small set of T1-weighted images (ranging from 0 to 50). When T2-weighted images were selected as the testing domain, ImageNet-trained and T1-trained networks were fine-tuned using a small set of T2-weighted images (ranging from 0 to 50). In both cases, the performance of fine-tuned networks was compared with the networks trained directly in the testing domain.

It is likely that the reconstruction performance of a fine-tuned network depends on both the number of images used for initial training and the number of images used for fine tuning. To examine the interaction between the number of training and fine-tuning samples, separate networks were trained using training sets of varying size between 500 to 4000. Each network was then fine-tuned using sets of size between 0 to 50. Reconstruction performance was evaluated to determine the number of fine-tuning samples that are required to achieve near-optimal performance for each separate size of training set.

NN-based reconstructions were also compared to those obtained by conventional CS. CS reconstructions were implemented via a nonlinear conjugate gradient method. Libraries in the SparseMRI V0.2 toolbox available at <https://people.eecs.berkeley.edu/~mlustig/Software.html> were used. Daubechies-4 wavelets were selected as the sparsifying transform, and the L1 regularization parameters was set to 10^{-3} . A total of 80 conjugate gradient iterations were used for the reconstruction of undersampled T1-weighted acquisitions, and 120 conjugate gradient iterations were used for the reconstruction of undersampled T2-weighted acquisitions.

To assess reconstruction quality, we used the structural similarity index measure (SSIM) and peak signal-to-noise ratio (PSNR) between the reconstructed and reference images. The training and testing of NN architectures were performed in the TensorFlow framework [28] using 2 nVidia Titan X Pascal GPUs (12 GB VRAM).

3 – Results

A network trained on the same type of images that it will later be tested on should outperform networks trained on different types of images than those in the test set. However, this performance difference should diminish following successful domain transfer between the training and testing domains. To test this prediction, we examined how well a network trained on a given dataset generalizes to other types of datasets. First, we investigated generalization performance when the testing domain contained T1-weighted images. Figure 2 displays reconstructions of an undersampled T1-weighted acquisition via the ImageNet-trained, T1-trained and T2-trained networks. As expected, the T1-trained network yields sharper and more accurate reconstructions compared to the ImageNet-trained and T2-trained networks (Fig. 2a). However, once the ImageNet-trained and T2-trained networks are fine-tuned using as few as 20 images, all reconstructions become of similar visual quality (Fig. 2b). Quantitative measurements of PSNR and SSIM are listed in Table 1. In the absence of fine tuning, ImageNet-trained, T2-trained networks and conventional CS yield comparable PSNR levels, approximately 2 dB lower than that of the T1-trained network. After fine tuning, the difference in PSNR between ImageNet-, T2-trained and T1-trained networks significantly diminishes.

Next, we examined the performance of NN-based reconstructions when the testing domain contained T2-weighted images. Figure 3 displays reconstructions of an undersampled T2-weighted acquisition via the ImageNet-trained, T1-trained and T2-trained networks. Again, the network trained directly in the testing domain (T2-weighted) outperforms those that are trained in other domains (ImageNet and T1-weighted). After fine tuning with as few as 20 images, the ImageNet-trained and T1-trained networks yield visually similar reconstructions to the T2-trained network (Fig. 3b). PSNR and SSIM measurements are listed in Table 2. PSNR difference between the ImageNet-trained and T1-trained networks prior to fine tuning is nearly 1 dB. Following domain transfer, fine-tuned networks trained on the ImageNet and T1-weighted datasets yield nearly identical reconstruction quality to the network directly trained on T2-weighted images.

Reconstruction performance of fine-tuned networks may depend on both the number of images used for initial training and the number of images used for fine tuning. To examine potential interactions between the number of training and fine-tuning samples, we trained networks using training sets in the range [500 4000] and fine-tuning sets in the range [0 50]. For T1-weighted acquisitions, Fig. 4 displays reconstructions via ImageNet-trained and T1-trained networks, and Table 3 lists the corresponding PSNR and SSIM values. As expected, the reconstruction quality is improved for all networks as the size of training dataset increases. However, for the ImageNet-trained network, the improvements due to the size of training data become less noticeable for larger number of fine-tuning samples. For the largest training set, the Image-Net trained network fine-tuned using 20 samples achieves nearly identical SSIM and a PSNR within 0.55 dB (nearly 6.5% difference in mean-squared error) of the T1-trained network fine-tuned using 50 samples.

Interaction between the number of training and fine-tuning samples was also examined for T2-weighted acquisitions. Figure 5 displays reconstructions via ImageNet-trained and T2-trained networks, and Table 4 lists the corresponding PSNR and SSIM values. In the absence of fine-tuning, the ImageNet-trained network yields lower reconstruction quality compared to the T2-trained network. With fine-tuning, the ImageNet-trained network achieves similar performance to the T2-trained network. For the largest training set, the

Image-Net trained network fine-tuned using 20 samples achieves nearly identical SSIM and a PSNR within 0.46 dB (nearly 5.4% difference in mean-squared error) of the T2-trained network fine-tuned using 50 samples.

Lastly, we compared NN-based reconstructions obtained via the proposed transfer-learning approach to those obtained via conventional CS reconstructions (Fig. 6). For reconstructions of both T1-weighted and T2-weighted acquisitions, the ImageNet-trained network produces images of similar visual quality to those produced by the networks trained directly in the testing domain. At the same time, ImageNet-trained networks outperform CS in terms of image sharpness and residual aliasing artifacts. On average, the proposed transfer-learning approach achieves 2.50 dB higher PSNR than CS for T1-weighted acquisitions, and 3.68 dB higher PSNR than CS for T2-weighted acquisitions. Furthermore, network-based reconstructions are computationally more efficient than iterative CS reconstructions. The total processing time for over 600 images contained in the test samples were 15 s (23 ms per image) with NN.

4 – Discussion

Neural network based architectures have recently been proposed for reconstruction of undersampled MR acquisitions [10]–[19]. These architectures involve many free parameters that must be learnt, so an extensive amount of training samples is typically needed [29]. Several previous studies trained deep neural networks on relatively large sized datasets by gathering single-contrast images from hundreds of subjects [14], [16], [17]. In theory, network performance should be optimized by drawing the training and testing samples from the same domain, ideally acquired under a common MRI protocol. In practice, however, compiling large datasets such as the brain images provided by HCP require coordinated efforts among multiple imaging centers, and therefore such datasets are rare. As an alternative, another study trained neural networks on multi-contrast images of the same anatomy from tens of subjects [19]. When needed, data augmentation procedures were used to further expand the training dataset [12], [14]. While this approach effectively increases the data size, it remains unclear how well a network trained on images acquired with a specific type of tissue contrast generalizes to images acquired with different contrasts. Thus, inherent variability in image properties across several contrasts can lead to suboptimal reconstruction performance.

Here, we propose a transfer-learning approach to address the problem of data scarcity in training deep neural networks for accelerated MRI. The proposed approach trains neural networks using training samples from a large public dataset of natural images (ImageNet). The trained network is then fine-tuned in the testing domain to transfer the knowledge gained during training. This transfer is achieved via end-to-end fine-tuning of the ImageNet-trained network using only few tens of MR images acquired in the testing domain. We show successful domain transfer between natural images (ImageNet) and MR images with two canonical contrasts (T1- or T2-weighted). Reconstructions obtained via the ImageNet-trained network are of nearly identical quality to reconstructions obtained by networks trained directly in the testing domain using thousands of MR images. Therefore, the proposed approach might facilitate the use of neural networks for MRI reconstruction in many applications.

Several recent studies considered domain transfer for neural-network based image reconstruction in MRI. In a previous study, Han et al. [11] trained a network to remove streaking artifacts from CT images, and the trained network was then used to suppress aliasing artifacts in projection-reconstruction MRI. Note that in this case a relatively large set of imaging data is still needed for network training. Another previous study instead used images from ImageNet to train a network that performs interpolation from a spiral to Cartesian sampling grid in the Fourier-domain. The trained network was then used to perform gridding reconstructions of spiral MR acquisitions [17]. Both studies inherently leveraged the characteristic structure of undersampling artifacts that arise in non-Cartesian sampling. However, random undersampling exercised in compressive sensing applications is designed to yield incoherent artifacts without an apparent structure.

To our knowledge this is the first study to address neural-network reconstructions of randomly undersampled MR acquisitions based on domain transfer between natural and MR images. Here, we demonstrated domain transfer based on a cascade architecture with multiple CNNs interleaved with data consistency layers. The proposed transfer-learning approach might also benefit other types of architectures that have been proposed for accelerated MRI [13], [15], [19], in particular architectures that require extensive datasets for adequate training [14], [16]. Note that the current study examined the generalization capability of networks trained on natural images to T1-weighted and T2-weighted images of

the brain. In future studies, we plan to test how well ImageNet-trained networks generalize to MR images acquired with more specific contrast such as angiograms, and to images acquired in other body parts.

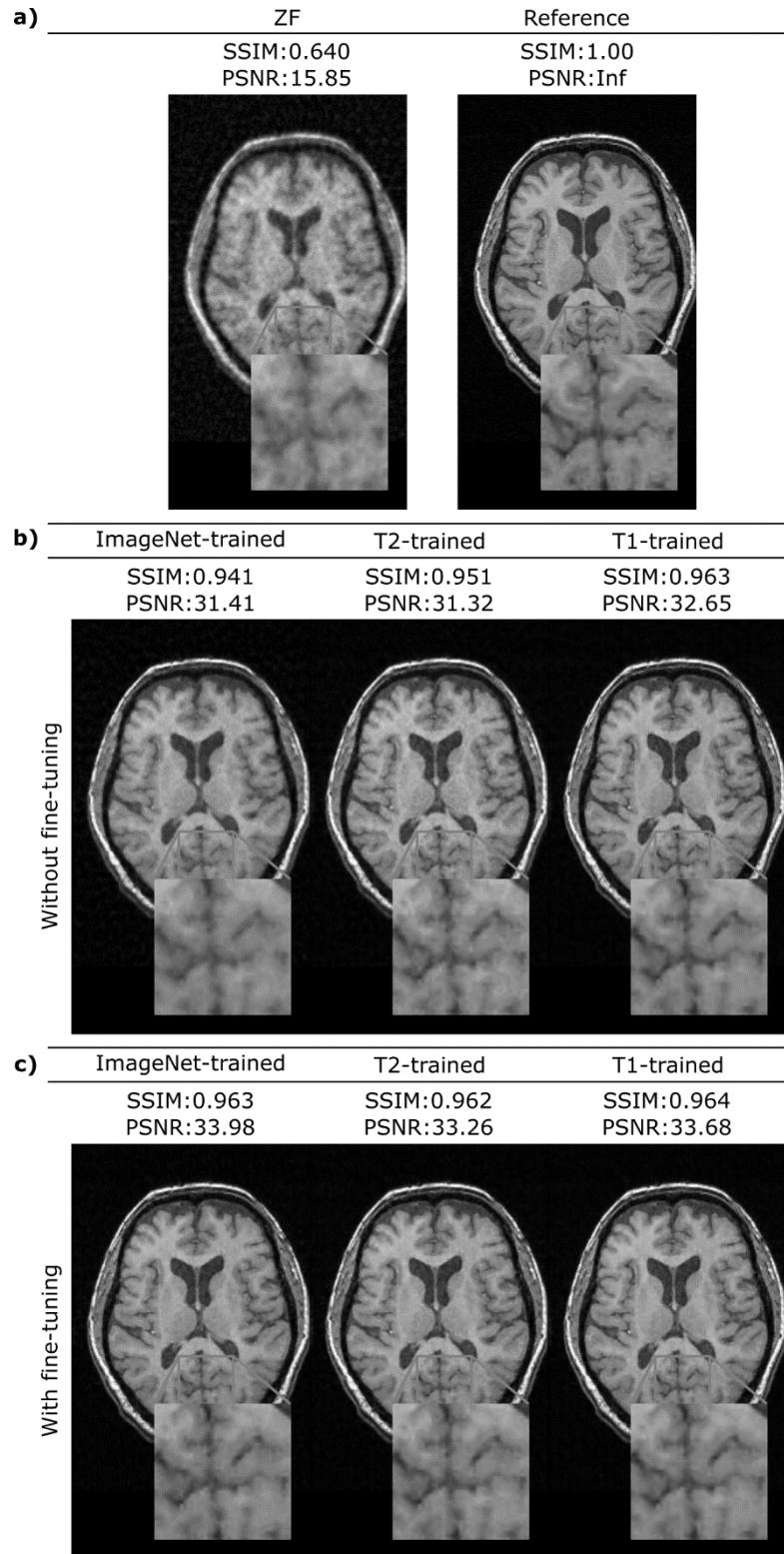


Figure 2. Representative reconstructions of a T1-weighted acquisition with 4-fold undersampling. (a) Zero-filled Fourier reconstructions (ZF) and the fully-sampled reference image. (b) Reconstructions via the ImageNet-trained, T2-trained and T1-trained networks. In each case, network training was performed on a training dataset of 4000 images. The ImageNet-trained and T2-trained networks yield suboptimal performance compared to a network trained directly on T1-weighted images. (c) Network reconstructions after fine-tuning on a sample of 20 T1-weighted images. Following fine-tuning with few tens of samples, ImageNet-trained and T2-trained networks yield reconstructions of similar quality to the T1-trained network.

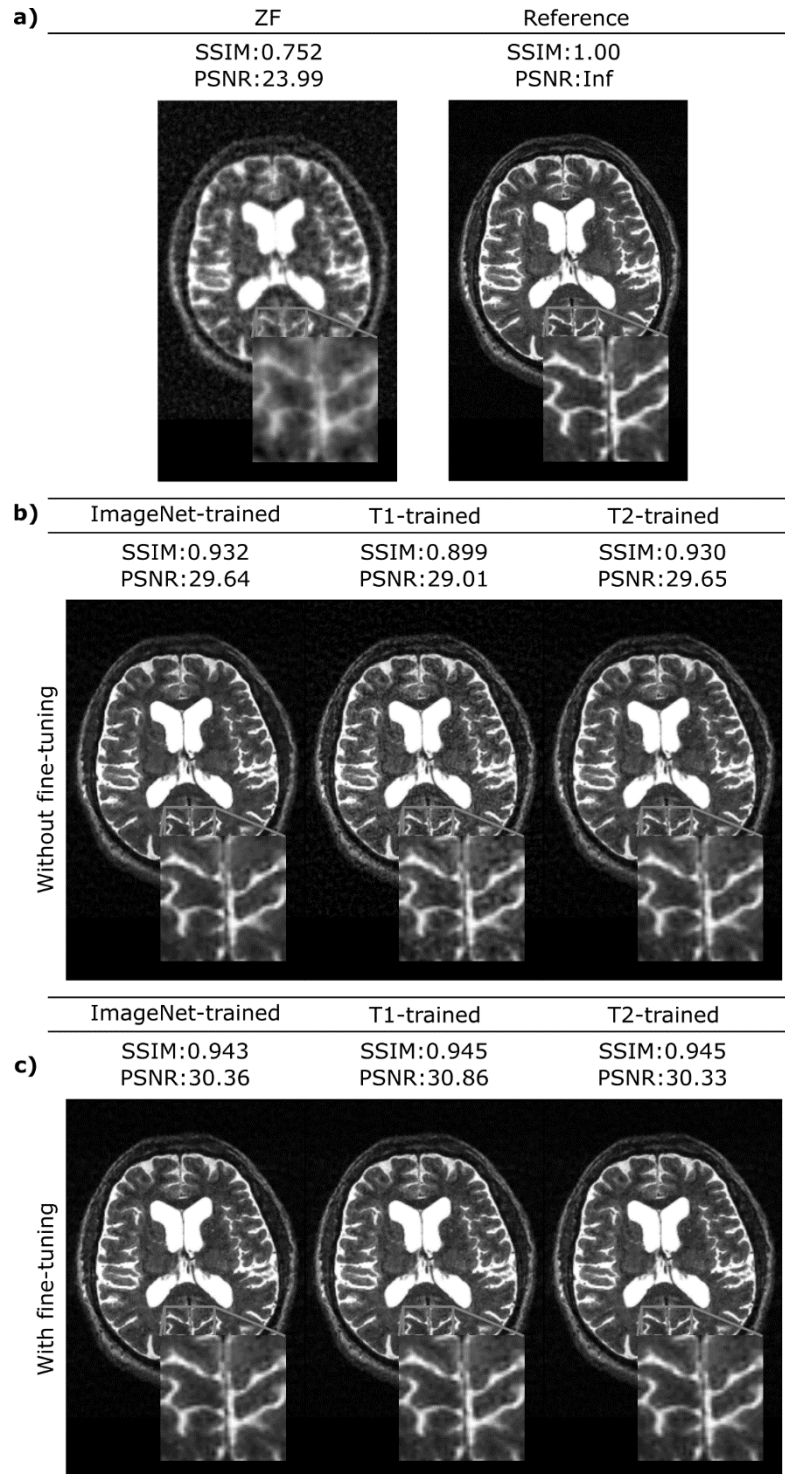


Figure 3. Representative reconstructions of a T2-weighted acquisition with 4-fold undersampling. (a) Zero-filled Fourier reconstructions (ZF) and the fully-sampled reference image. (b) Reconstructions via the ImageNet-trained, T1-trained and T2-trained networks. In each case, network training was performed on a training dataset of 4000 images. The ImageNet-trained and T1-trained networks can yield suboptimal performance compared to a network trained directly on T2-weighted images. (c) Network reconstructions after fine-tuning on a sample of 20 T2-weighted images. Following fine-tuning with few tens of samples, ImageNet-trained and T1-trained networks yield reconstructions of similar quality to the T2-trained network.

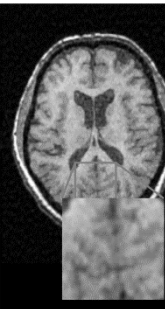
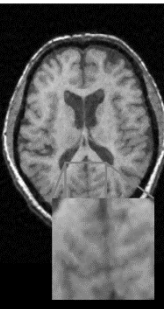
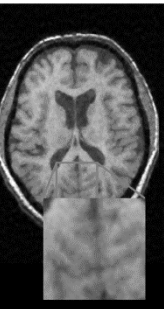
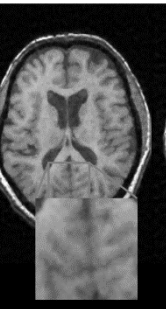
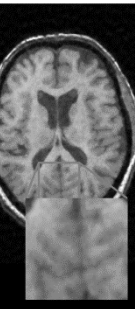
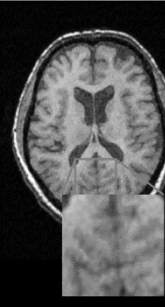
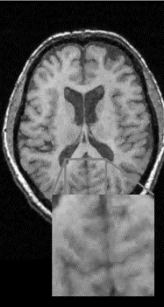
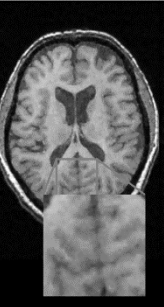
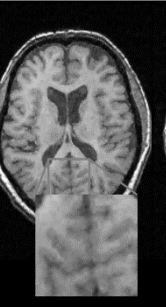
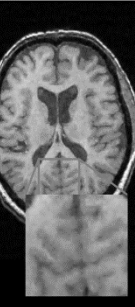
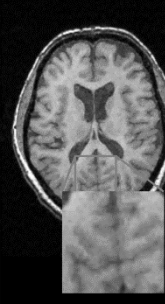
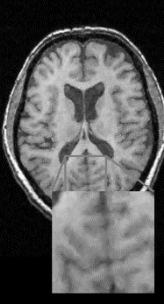
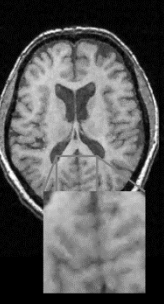
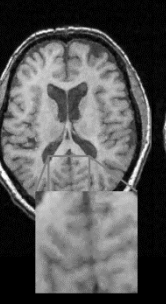
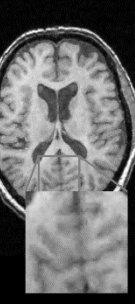
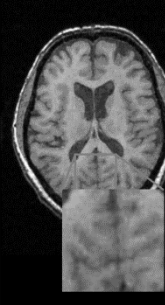
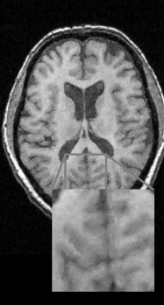
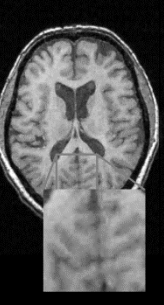
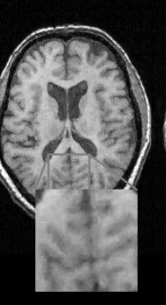
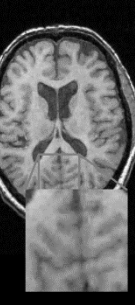
		Number of images used for training				
		500	1000	1500	2000	4000
		SSIM:0.887 PSNR:24.91	SSIM:0.930 PSNR:27.85	SSIM:0.927 PSNR:28.39	SSIM:0.937 PSNR:29.75	SSIM:0.934 PSNR:30.95
No fine-tuning						
		SSIM:0.933 PSNR:28.23	SSIM:0.952 PSNR:30.78	SSIM:0.954 PSNR:31.36	SSIM:0.956 PSNR:31.94	SSIM:0.958 PSNR:33.50
Fine-tuning on 5 images						
		SSIM:0.950 PSNR:31.05	SSIM:0.958 PSNR:33.12	SSIM:0.958 PSNR:32.59	SSIM:0.959 PSNR:33.06	SSIM:0.960 PSNR:33.75
Fine-tuning on 20 images						
		SSIM:0.949 PSNR:31.28	SSIM:0.957 PSNR:32.39	SSIM:0.958 PSNR:32.93	SSIM:0.958 PSNR:32.70	SSIM:0.962 PSNR:33.92
T1-trained network						

Figure 4. An ImageNet-trained network was trained on a dataset of natural images, and then fine-tuned on a small dataset of T1-weighted images. This network was used to reconstruct a 4-fold undersampled T1-weighted acquisition. Reconstructions are shown for varying training dataset sizes in [500 4000] and fine-tuning dataset sizes of [0 20]. Reference reconstructions from a network trained directly on T1-weighted images without fine-tuning are also shown (bottom row). In the absence of fine-tuning, the ImageNet-trained network yields lower reconstruction quality compared to the T1-trained network. With fine-tuning, the ImageNet-trained network achieves similar performance to the T1-trained network. As expected, the reconstruction quality is improved for all networks as the size of training dataset increases. However, for the ImageNet-trained network, the improvements due to the size of training data become less noticeable for larger number of fine-tuning samples.

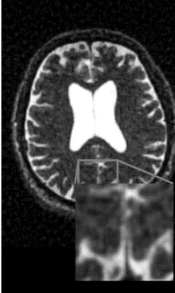


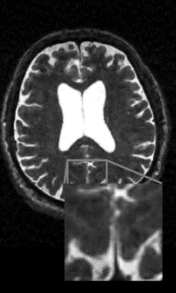

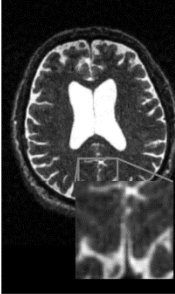




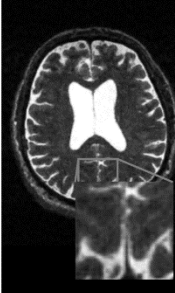




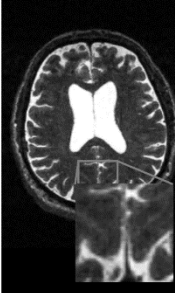



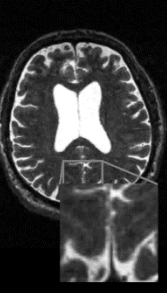
		Number of images used for training				
		500	1000	1500	2000	4000
		SSIM:0.877 PSNR:27.78	SSIM:0.930 PSNR:30.20	SSIM:0.936 PSNR:31.07	SSIM:0.941 PSNR:31.75	SSIM:0.945 PSNR:32.18
No fine-tuning						
		SSIM:0.930 PSNR:30.27	SSIM:0.947 PSNR:31.84	SSIM:0.949 PSNR:32.26	SSIM:0.949 PSNR:32.39	SSIM:0.950 PSNR:32.61
Fine-tuning on 5 images						
		SSIM:0.946 PSNR:32.02	SSIM:0.952 PSNR:32.65	SSIM:0.953 PSNR:32.36	SSIM:0.953 PSNR:32.73	SSIM:0.954 PSNR:32.93
Fine-tuning on 20 images						
		SSIM:0.953 PSNR:32.64	SSIM:0.952 PSNR:32.54	SSIM:0.956 PSNR:32.95	SSIM:0.955 PSNR:32.96	SSIM:0.956 PSNR:33.09
T2-trained network						

Figure 5. An ImageNet-trained network was trained on a dataset of natural images, and then fine-tuned on a small dataset of T2-weighted images. This network was used to reconstruct a 4-fold undersampled T2-weighted acquisition. Reconstructions are shown for varying training dataset sizes in [500 4000] and fine-tuning dataset sizes of [0 20]. Reference reconstructions from a network trained directly on T2-weighted images without fine-tuning are also shown (bottom row). In the absence of fine-tuning, the ImageNet-trained network yields lower reconstruction quality compared to the T2-trained network. After fine-tuning, the ImageNet-trained network achieves similar performance to the T2-trained network. As expected, the reconstruction quality is improved for all networks as the size of training dataset increases. However, for the ImageNet-trained network, the improvements due to the size of training data become less noticeable for larger number of fine-tuning samples.

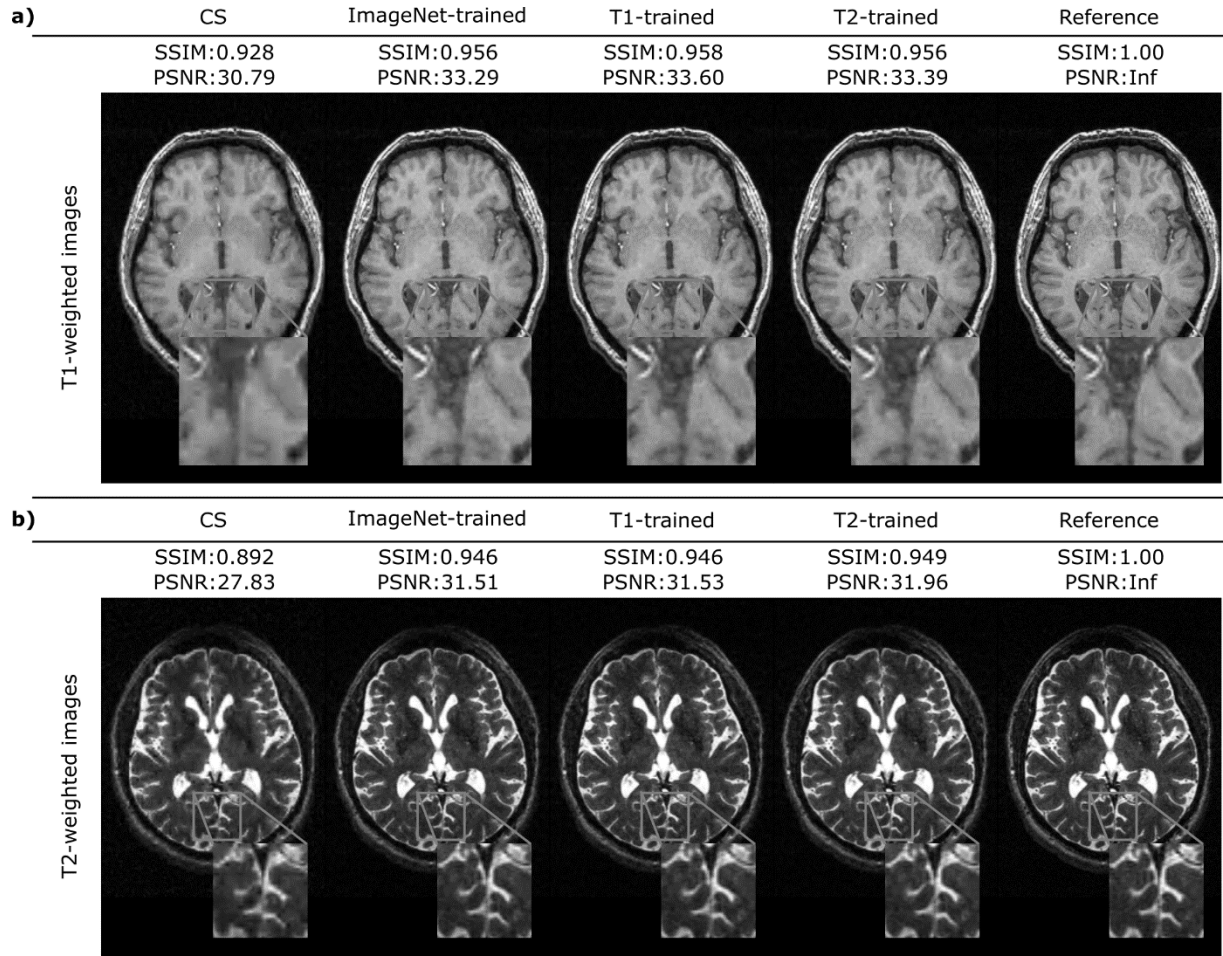


Figure 6. (a) Reconstructions of a T1-weighted acquisition with 4-fold undersampling via a conventional compressed-sensing method (CS), and ImageNet-trained, T1-trained, T2-trained networks along with the fully-sampled reference image. (b) Reconstructions of a T2-weighted acquisition with 4-fold undersampling via CS, and ImageNet-trained, T1-trained, T2-trained networks along with the fully-sampled reference image. Networks were trained on 4000 images and fine-tuned on 20 images acquired with the test contrast. The ImageNet-trained network maintain similar performance to the networks trained directly on the test images. Furthermore, the ImageNet-based reconstructions outperform conventional CS in terms of image sharpness and residual aliasing artifacts.

Table 1. Performances of the ImageNet-trained, T1-trained and T2-trained networks were assessed on a test dataset of 628 T1-weighted images. SSIM and PSNR values are reported as mean \pm standard deviation. The networks were trained using separate datasets of 4000 images. Results are shown for both networks obtained after training (raw), and fine-tuned networks using 20 sample T1-weighted images (tuned). SSIM and PSNR measurements for conventional compressed-sensing (CS) are also reported.

	ImageNet-trained		T1-trained		T2-trained	
	<i>SSIM</i>	<i>PSNR</i>	<i>SSIM</i>	<i>PSNR</i>	<i>SSIM</i>	<i>PSNR</i>
Raw	0.949 \pm .022	33.44 \pm 3.43	0.967 \pm .014	35.42 \pm 2.52	0.962 \pm .022	34.42 \pm 3.06
Tuned	0.967 \pm .015	35.59 \pm 2.72	0.969 \pm .014	35.89 \pm 2.63	0.967 \pm .015	35.68 \pm 2.73
CS						
<i>SSIM</i>				<i>PSNR</i>		
0.947 \pm .022				33.36 \pm 3.31		

Table 2. Performances of the ImageNet-trained, T1-trained and T2-trained networks were assessed on a test dataset of 640 T2-weighted images. SSIM and PSNR values are reported as mean \pm standard deviation. The networks were trained using separate datasets of 4000 images. Results are shown for both networks obtained after training (raw), and fine-tuned networks using 20 sample T2-weighted images (tuned). SSIM and PSNR measurements for conventional compressed-sensing (CS) are also reported.

	ImageNet-trained		T1-trained		T2-trained	
	<i>SSIM</i>	<i>PSNR</i>	<i>SSIM</i>	<i>PSNR</i>	<i>SSIM</i>	<i>PSNR</i>
Raw	0.957 \pm .012	33.86 \pm 1.83	0.943 \pm .017	33.22 \pm 2.03	0.962 \pm .012	34.90 \pm 2.03
Tuned	0.965 \pm .010	35.20 \pm 1.85	0.966 \pm .010	35.29 \pm 1.89	0.967 \pm .010	35.51 \pm 1.87
CS						
<i>SSIM</i>				<i>PSNR</i>		
0.935 \pm .019				31.98 \pm 2.14		

Table 3. The performance of the ImageNet-trained network was assessed on a test dataset of 628 T1-weighted images. SSIM and PSNR values are reported as mean \pm standard deviation. The number of samples used for training the networks ranged from 500 to 4000. The networks were fine-tuned using [0 50] sample T1-weighted images. The performance of a reference T1-trained network is also listed (bottom row).

No. of samples for fine tuning	No. of samples for training				
	500	1000	1500	2000	4000
	<i>SSIM</i>				
0	0.884 \pm .038	0.944 \pm .022	0.944 \pm .023	0.951 \pm .021	0.949 \pm .022
5	0.938 \pm .024	0.961 \pm .016	0.962 \pm .016	0.965 \pm .016	0.966 \pm .015
10	0.949 \pm .019	0.964 \pm .015	0.964 \pm .016	0.966 \pm .016	0.967 \pm .015
20	0.957 \pm .016	0.965 \pm .015	0.965 \pm .015	0.966 \pm .015	0.967 \pm .015
30	0.962 \pm .015	0.967 \pm .015	0.967 \pm .015	0.968 \pm .015	0.968 \pm .015
40	0.965 \pm .015	0.968 \pm .015	0.968 \pm .015	0.968 \pm .015	0.969 \pm .015
50	0.966 \pm .015	0.969 \pm .014	0.969 \pm .015	0.969 \pm .015	0.969 \pm .014
T1-trained	0.966 \pm .015	0.968 \pm .014	0.966 \pm .014	0.969 \pm .014	0.970 \pm .014
	<i>PSNR</i>				
0	25.91 \pm 3.50	31.05 \pm 3.54	31.94 \pm 3.69	33.30 \pm 3.47	33.44 \pm 3.43
5	30.01 \pm 3.46	33.89 \pm 2.75	33.90 \pm 2.83	34.93 \pm 2.76	35.16 \pm 2.66
10	31.66 \pm 3.19	34.77 \pm 2.70	34.83 \pm 2.74	35.26 \pm 2.81	35.58 \pm 2.78
20	33.16 \pm 2.91	35.03 \pm 2.65	34.99 \pm 2.75	35.24 \pm 2.72	35.59 \pm 2.72
30	34.29 \pm 2.76	35.42 \pm 2.66	35.40 \pm 2.83	35.57 \pm 2.75	35.76 \pm 2.74
40	34.83 \pm 2.70	35.55 \pm 2.60	35.58 \pm 2.81	35.68 \pm 2.74	35.88 \pm 2.74
50	35.26 \pm 2.67	35.77 \pm 2.63	35.79 \pm 2.84	35.86 \pm 2.77	36.02 \pm 2.77
T1-trained	35.13 \pm 2.77	35.63 \pm 2.62	34.69 \pm 2.32	35.81 \pm 2.64	36.14 \pm 2.68

Table 4. The performance of the ImageNet-trained network was assessed on a test dataset of 640 T2-weighted images. SSIM and PSNR values are reported as mean \pm standard deviation. The number of samples used for training the networks ranged from 500 to 4000. The networks were fine-tuned using [0 50] sample T2-weighted images. The performance of a reference T2-trained network is also listed (bottom row).

No. of samples for fine tuning	No. of samples for training				
	500	1000	1500	2000	4000
	<i>SSIM</i>				
0	0.887 \pm 0.022	0.947 \pm 0.014	0.951 \pm 0.013	0.954 \pm 0.012	0.957 \pm 0.012
5	0.949 \pm 0.013	0.960 \pm 0.011	0.961 \pm 0.011	0.962 \pm 0.011	0.962 \pm 0.011
10	0.955 \pm 0.012	0.961 \pm 0.011	0.962 \pm 0.011	0.962 \pm 0.011	0.963 \pm 0.011
20	0.960 \pm 0.011	0.964 \pm 0.011	0.965 \pm 0.010	0.964 \pm 0.011	0.965 \pm 0.010
30	0.962 \pm 0.011	0.965 \pm 0.010	0.965 \pm 0.010	0.965 \pm 0.010	0.966 \pm 0.010
40	0.963 \pm 0.011	0.965 \pm 0.010	0.966 \pm 0.010	0.965 \pm 0.010	0.966 \pm 0.010
50	0.964 \pm 0.011	0.966 \pm 0.010	0.966 \pm 0.010	0.966 \pm 0.010	0.967 \pm 0.010
T2-trained	0.966 \pm 0.010	0.966 \pm 0.010	0.968 \pm 0.010	0.967 \pm 0.010	0.968 \pm 0.010
	<i>PSNR</i>				
0	28.41 \pm 1.74	32.77 \pm 1.80	33.32 \pm 1.72	33.68 \pm 1.82	33.86 \pm 1.83
5	32.54 \pm 1.80	34.14 \pm 1.90	34.48 \pm 1.87	34.46 \pm 1.92	34.66 \pm 1.88
10	33.38 \pm 1.85	34.39 \pm 1.93	34.71 \pm 1.91	34.60 \pm 1.94	34.82 \pm 1.89
20	34.26 \pm 1.82	34.91 \pm 1.86	35.06 \pm 1.82	34.99 \pm 1.83	35.20 \pm 1.85
30	34.63 \pm 1.84	35.13 \pm 1.85	35.20 \pm 1.82	35.15 \pm 1.82	35.34 \pm 1.84
40	34.80 \pm 1.84	35.21 \pm 1.84	35.28 \pm 1.81	35.22 \pm 1.81	35.30 \pm 1.84
50	34.97 \pm 1.83	35.28 \pm 1.83	34.36 \pm 1.80	35.28 \pm 1.80	35.43 \pm 1.83
T2-trained	35.35 \pm 1.85	35.29 \pm 1.87	35.59 \pm 1.84	35.55 \pm 1.86	35.66 \pm 1.86

References

- [1] K. T. Block, M. Uecker, and J. Frahm, "Undersampled radial MRI with multiple coils. Iterative image reconstruction using a total variation constraint," *Magn. Reson. Med.*, vol. 57, no. 6, pp. 1086–1098, 2007.
- [2] M. Lustig, D. Donoho, and J. M. Pauly, "Sparse MRI: The application of compressed sensing for rapid MR imaging," *Magn. Reson. Med.*, vol. 58, no. 6, pp. 1182–1195, 2007.
- [3] T. Çukur, M. Lustig, and D. G. Nishimura, "Improving non-contrast-enhanced steady-state free precession angiography with compressed sensing," *Magn. Reson. Med.*, vol. 61, no. 5, pp. 1122–1131, 2009.
- [4] H. Jung and J. C. Ye, "Performance evaluation of accelerated functional MRI acquisition using compressed sensing," in *IEEE International Symposium on Biomedical Imaging: From Nano to Macro*, 2009, pp. 702–705.
- [5] M. I. Menzel *et al.*, "Accelerated diffusion spectrum imaging in the human brain using compressed sensing," *Magn. Reson. Med.*, vol. 66, no. 5, pp. 1226–1233, 2011.
- [6] M. Doneva, P. Börnert, H. Eggers, C. Stehning, J. Sénagás, and A. Mertins, "Compressed sensing reconstruction for magnetic resonance parameter mapping," *Magn. Reson. Med.*, vol. 64, no. 4, pp. 1114–1120, 2010.
- [7] S. Ravishankar and Y. Bresler, "MR image reconstruction from highly undersampled k-space data by dictionary learning," *IEEE Trans. Med. Imaging*, vol. 30, no. 5, pp. 1028–1041, 2011.
- [8] K. Khare, C. J. Hardy, K. F. King, P. A. Turski, and L. Marinelli, "Accelerated MR imaging using compressive sensing with no free parameters," *Magn. Reson. Med.*, vol. 68, no. 5, pp. 1450–1457, 2012.
- [9] D. S. Weller, S. Ramani, J.-F. Nielsen, and J. A. Fessler, "Monte Carlo SURE-based parameter selection for parallel magnetic resonance imaging reconstruction," *Magn. Reson. Med.*, vol. 71, no. 5, pp. 1760–1770, 2014.
- [10] S. Wang *et al.*, "ACCELERATING MAGNETIC RESONANCE IMAGING VIA DEEP LEARNING," in *IEEE 13th International Symposium on Biomedical Imaging (ISBI)*, 2016, pp. 514–517.
- [11] Y. S. Han, J. Yoo, and J. C. Ye, "Deep Learning with Domain Adaptation for Accelerated Projection Reconstruction MR," *arXiv Prepr.*, 2017.
- [12] J. Schlemper, J. Caballero, J. V. Hajnal, A. Price, and D. Rueckert, "A Deep Cascade of Convolutional Neural Networks for MR Image Reconstruction," *arXiv Prepr.*, 2017.
- [13] K. Hammernik *et al.*, "Learning a Variational Network for Reconstruction of Accelerated MRI Data," *arXiv Prepr.*, 2017.
- [14] S. Yu *et al.*, "Deep De-Aliasing for Fast Compressive Sensing MRI," *arXiv Prepr.*, 2017.
- [15] Y. Yang, J. Sun, H. Li, and Z. Xu, "ADMM-Net: A Deep Learning Approach for Compressive Sensing MRI," *arXiv Prepr.*, 2017.
- [16] M. Mardani *et al.*, "Deep Generative Adversarial Networks for Compressed Sensing Automates MRI," *arXiv Prepr.*, 2017.
- [17] B. Zhu, J. Z. Liu, B. R. Rosen, and M. S. Rosen, "Image reconstruction by domain transform manifold learning," *arXiv Prepr.*, 2017.

- [18] T. M. Quan, T. Nguyen-Duc, and W.-K. Jeong, "Compressed Sensing MRI Reconstruction with Cyclic Loss in Generative Adversarial Networks," pp. 1–10, 2017.
- [19] C. M. Hyun, H. P. Kim, S. M. Lee, S. Lee, and J. K. Seo, "Deep learning for undersampled MRI reconstruction," no. 1, pp. 1–11, 2017.
- [20] A. Krizhevsky, I. Sutskever, and G. E. Hinton, "ImageNet Classification with Deep Convolutional Neural Networks," in *Advances in Neural Information Processing Systems 25*, F. Pereira, C. J. C. Burges, L. Bottou, and K. Q. Weinberger, Eds. Curran Associates, Inc., 2012, pp. 1097–1105.
- [21] J. Donahue *et al.*, "DeCAF: A Deep Convolutional Activation Feature for Generic Visual Recognition," in *Proceedings of the 31st International Conference on Machine Learning*, 2014, vol. 32, no. 1, pp. 647–655.
- [22] J. Yosinski, J. Clune, Y. Bengio, and H. Lipson, "How transferable are features in deep neural networks?," in *Advances in Neural Information Processing Systems 27*, Z. Ghahramani, M. Welling, C. Cortes, N. D. Lawrence, and K. Q. Weinberger, Eds. Curran Associates, Inc., 2014, pp. 3320–3328.
- [23] O. Russakovsky *et al.*, "ImageNet Large Scale Visual Recognition Challenge," *Int. J. Comput. Vis.*, vol. 115, no. 3, pp. 211–252, 2015.
- [24] E. Bullitt *et al.*, "Vessel tortuosity and brain tumor malignancy: A blinded study," in *Academic Radiology*, 2005, vol. 12, no. 10, pp. 1232–1240.
- [25] M. Lustig and J. M. Pauly, "SPIRiT: Iterative self-consistent parallel imaging reconstruction from arbitrary k-space," *Magn. Reson. Med.*, vol. 64, no. 2, pp. 457–471, 2010.
- [26] D. E. Rumelhart, G. E. Hinton, and R. J. Williams, "Learning representations by back-propagating errors," *Nature*, vol. 323, no. 6088, pp. 533–536, 1986.
- [27] D. P. Kingma and J. L. Ba, "Adam: a Method for Stochastic Optimization," *Int. Conf. Learn. Represent. 2015*, pp. 1–15, 2015.
- [28] M. Abadi *et al.*, "TensorFlow: Large-Scale Machine Learning on Heterogenous Distributed Systems," in *12th USENIX Symposium on Operating Systems Design and Implementation (OSDI '16)*, 2016, pp. 265–284.
- [29] P. Domingos, "A few useful things to know about machine learning," *Commun. ACM*, vol. 55, no. 10, p. 78, 2012.